



TanSat Mission Achievements: from Scientific Driving to Preliminary Observations

LIU Yi^{1, 2}, WANG Jing^{1, 2}, YAO Lu^{1, 2}, CHEN Xi^{1, 2}, CAI Zhaonan¹,
YANG Dongxu¹, YIN Zengshan³, GU Songyan⁴, TIAN Longfei³,
LU Naimeng⁴, LÜ Daren¹

1. (Institute of Atmospheric Physics, Chinese Academy of Sciences)
2. (University of Chinese Academy of Sciences)
3. (Shanghai Engineering Center for Microsatellites)
4. (National Satellite Meteorological Center, China Meteorological Administration)

Abstract

The Chinese global carbon dioxide monitoring satellite (TanSat) was successfully launched in December 2016 and has completed its on-orbit tests and calibration. TanSat aims to measure the atmospheric Carbon Dioxide column-averaged dry air mole fractions (X_{CO_2}) with a precision of 4 ppm at the regional scale, and further to derive the CO_2 global and regional fluxes. Progress toward these objectives is reviewed and the first scientific results from TanSat measurements are presented. During the design phase, Observation System Simulation Experiments (OSSE) on TanSat measurements performed prior to launch measurements using a nadir and a glint alternative mode when considering the balance of stable measurements and reduces the flux uncertainty (64%). The constellation measurements of two satellites indicate an extra 10% improvement in flux inversion if the satellite measurements have no bias and similar precision.

The TanSat on-orbit test indicates that the instrument is stable and beginning to produce X_{CO_2} products. The preliminary TanSat measurements have been validated with Total Carbon Column Observing Network (TCCON) measurements and have inter-compared with OCO-2 measurements in an overlap measurement. The first scientific achievements are presented as the seasonal distributions of X_{CO_2} at the global scale.

Key words

TanSat; Carbon dioxide; Retrieval algorithm; Carbon flux inversion

1. Introduction

Carbon Dioxide (CO_2) can be released into the atmosphere by anthropogenic activity and biological respiration, while it is absorbed from the atmosphere by processes at both land surface and ocean, such as photosynthesis from vegetation. Since the beginning of the industrial age, humans have disrupted the carbon balance through the use of fossil fuels and deforestation. It is well known that the increase in atmospheric CO_2 has resulted in global warming and subsequently, climate change.

Many ground-based stations make up the networks to

observe atmospheric CO_2 concentration from the surface, offering accurate CO_2 measurements around the world. Compared with in-situ observations, monitoring atmospheric CO_2 from space using the Near Infrared (NIR) and ShortWave Infrared (SWIR) spectra can provide the global distribution of CO_2 with high accuracy and precision to improve our understanding of CO_2 fluxes (sources and sinks). One of the main approaches to inverse surface carbon flux, called a top-down method, tries to assimilate the column CO_2 concentration measurements to constrain surface CO_2 flux. From the distribution of surface CO_2 flux, the understanding of carbon cycle in the atmosphere is improved. The first

satellite that used atmospheric carbon dioxide column-averaged dry air mole fractions (X_{CO_2}) measurement is the Scanning Imaging Absorption Spectrometer for Atmospheric Chartography (SCIAMACHY) onboard ESA ENVISAT^[1-3]. A new generation instrument and satellite is required for future greenhouse gas monitoring. In 2009, the Japanese Greenhouse Observing Satellite (GOSAT) was launched successfully and has become the first greenhouse gas monitoring satellite with an on-orbit operation time of more than 8 years^[4-6]. Following this, the NASA Orbiting Carbon Observatory 2 (OCO-2) was launched in July 2014^[7-9].

Studies on the assimilation of GOSAT data using different inverse models and different retrieval algorithms have investigated the impact of satellite measurements on the CO_2 surface flux estimation. Results have proven that GOSAT data significantly improves our knowledge of the CO_2 surface fluxes over terrestrial vegetated areas^[10,11]. The Observation System Simulation Experiment (OSSE) on OCO measurement also indicated consistent results^[12]. However, in flux inversion, regional biases of a few tenths of a part per million in X_{CO_2} can result in the inverted yearly sub-continental fluxes being biased by a few-tenths of a Giga ton of carbon^[13-15]. Simulation studies indicate that the measurements from space can improve the CO_2 flux estimate significantly if they meet the accuracy and precision requirements^[16]. Therefore, the accuracy and precision of measurements from space is a critical constraint in satellite design and manufacture.

As the largest developing country, China faces a serious problem of GreenHouse Gas (GHG) emissions. To pursue sustainable development and reduce GHG emissions, quantification of the carbon budget at global and regional scales is critical and has become a significant challenge. The Chinese Global Carbon Dioxide Monitoring Scientific Experimental Satellite (TanSat) was established by the National High Technology Research and Development Program of China (863 Program). The main objective of the TanSat is to monitor the X_{CO_2} distribution and CO_2 flux at the regional and global scale^[17,18]. Since December 2016, TanSat has been launched successfully and commenced on-orbit tests and calibration.

In this paper, we introduce the scientific aspects and requirements of the TanSat mission. This starts with a brief introduction of the engineering process in terms of instrument design, measurement, data receiving, and

processing, as well as the operational retrieval algorithm in Section 2. The OSSE before TanSat launch is described in Section 3. Since the TanSat has been launched in 2016, we show the preliminary results of TanSat measurements in Section 4. Finally, we discuss the outlook of TanSat mission and future possible cooperation.

2. TanSat Mission

2.1 Instruments and Requirements

The TanSat is an agile satellite platform deployed in a sun-synchronous orbit, which operates in three observation modes, including nadir mode, sun-glint mode, and target mode. Nadir mode is the common observation mode over the land surface, in which the instrument records data along the satellite ground track. The ocean surface has low surface reflectance and hence, nadir mode cannot yield high precision measurements due to low Signal to Noise Ratio (SNR). To deal with this problem, the satellite tracks the sun glint spot, where sunlight is reflected specularly from the ocean, with the instrument boresight pointed within five degrees of the principal plane. TanSat also has a target mode which observes a stationary surface target as the satellite flies overhead. The main purpose of target mode is to validate with in-situ observation, but it also has the capability to get multi-angle (-60° to 60°) observations over one surface target and investigating the emission of hot spots. These measurements also can be compared with ground-based observations in order to validate the quality of CO_2 measurement from space. There are two scientific instruments onboard the TanSat, including a hyperspectral grating spectrometer (Atmospheric Carbon dioxide Grating Spectrometer (ACGS)) and a moderate resolution imaging polarization spectroradiometer (Cloud and Aerosol Polarization Imager (CAPI)).

2.1.1 ACGS and Requirements

ACGS is the primary instrument that is designed to measure the NIR/SWIR backscattered sunlight in the molecular oxygen (O_2) A-band ($0.76 \mu m$) and two CO_2 bands (1.61 and $2.06 \mu m$). The information about the total column of CO_2 is mainly from the measurement of absorption lines of CO_2 in the weak band ($1.61 \mu m$). The sunlight was significantly scattered and absorbed by air molecules and suspended particles (e.g. cloud and aerosol), while the equivalent light path impact by single and multi-scatters results in serious errors in retrieval. Following the approach pioneered by the

SCIAMACHY, GOSAT, and OCO-2 teams, independently approaching CO₂ from the weak band measurement cannot avoid this interference. More information on cloud and aerosol measurements is required in retrieval to correct the light path. Therefore, the XCO₂ is transferred from total column to concentration by a light path correction factor, which is represented by surface pressure as follows:

$$XCO_2 = \frac{\int_{p_0}^0 [n_{CO_2}(p)]_p dp}{\int_{p_0}^0 [n_{air}(p)]_p dp} \quad (1)$$

Where n_{CO_2} and n_{air} is the mole fraction of CO₂ and dry air, while square brackets indicate the mole fraction per unit dry pressure variation. The integration actually represents the total column of CO₂ and dry air. The surface pressure p_0 is satisfied by both the O₂-A and CO₂ bands at the same time, which means that the cloud and aerosol interferences correction are harmonious to all bands. The majority of the information of aerosol and cloud altitude and the total amount (aerosol optical depth) are obtained from the O₂-A band due to the O₂ content being almost constant and stable^[19]. In comparison, the absorption of inference from water vapor is relatively weak. However, the CO₂ weak band is far away from O₂-A band in wavelength and aerosol and cloud optical properties can change with wavelength. One of the contributions of the CO₂ strong band is to constrain this variation. The CO₂ strong band also provides information on water vapor and temperature, which reduces the impact of uncertainties in these parameters.

The design of the optical system layout of ACGS and the specifications of instrument optical parameters can be found in Lin *et al.* (2017)^[20]. The footprint is 2 × 2 km in the nadir mode with nine footprints in each swath, while the total width of FOV is 18 km. Liu *et al.* (2014)^[21] have discussed the impact of spectral resolution and under-sampling effect on XCO₂ retrieval precision introduced by the use of a 500-pixel detector in both CO₂ weak and strong bands. Finally, we decided to reduce the spectral resolution to satisfy the sampling rate, and hence the SNR is better than in the previous design^[22]. We simulated the calibration accuracy from the references of scientific and engineering requirements. We used the Bayes based linear analysis of Optimal Estimation Method (OEM) to evaluate the calibration impact on XCO₂ retrieval precision. The radiometric calibration is the most important for guaranteeing that the meas-

urement is good enough for XCO₂ retrieval. Figure 1 indicates the absolute and relative calibration accuracy related to XCO₂ retrieval precision in four solar zenith angles. As this considers the TanSat observation over the land, most of the measurements are completed in the nadir mode and are extremely close to the perpendicular measurement to the land surface. Thus, only nadir geometry is simulated in this study. The results indicate that the relative radiometric calibration requires more accuracy rather than absolute values as the relative radiometric calibration is more sensitive to the relative change of absorption online/offline ratio describing the CO₂ concentration. At small Solar Zenith Angles (SZA), the XCO₂ error pattern changed from 15° to 50°. As the SZA increased from 50° to 70°, the absolute radiometric calibration accuracy becomes more critical for XCO₂ errors. Unlike the noise and relative radiometric calibrations, the absolute radiometric calibration introduces a linear bias as a systematic error in CO₂ retrieval in this simulated study.

The Instrument Line Shape (ILS) is important to describe the absorption lines in instrument resolution and sampling characteristics. To assess the dependence on ILS calibration, pre-launch simulations assumed that the ILS can be described by a Gaussian profile. Hence, there are two parameters in describing the ILS, including the peak position and Full Width at Half Maximum (FWHM). In the TanSat spectral calibration simulation experiment, we investigated the impact of peak position and FWHM calibration accuracy on XCO₂ retrieval errors. The following assumptions are included in the simulation: (1) the ILS shape was identical to the same Gaussian profile and FWHM, and (2) the error of peak position only results in the shift and there is no shift correction in retrieval. We used FWHM as a reference to measure the errors of peak position and FWHM (Figure 2). The results indicate that we need a very high accuracy for both peak position and FWHM in calibration. For example, the precision of 1 ppm on XCO₂ retrieval requires an accuracy of 1% (FWHM) on both peak position and FWHM. If the calibration accuracy of peak position is larger than 5% (FWHM) or if FWHM is larger than 9%, the XCO₂ error is never less than 4 ppm.

2.1.2 CAPI and Requirements

One of the most significant impacts on XCO₂ retrieval accuracy is scattering from aerosol and cirrus^[23,24]. The information for aerosol and cloud given in the spectra themselves are limited and need to be improved in CO₂

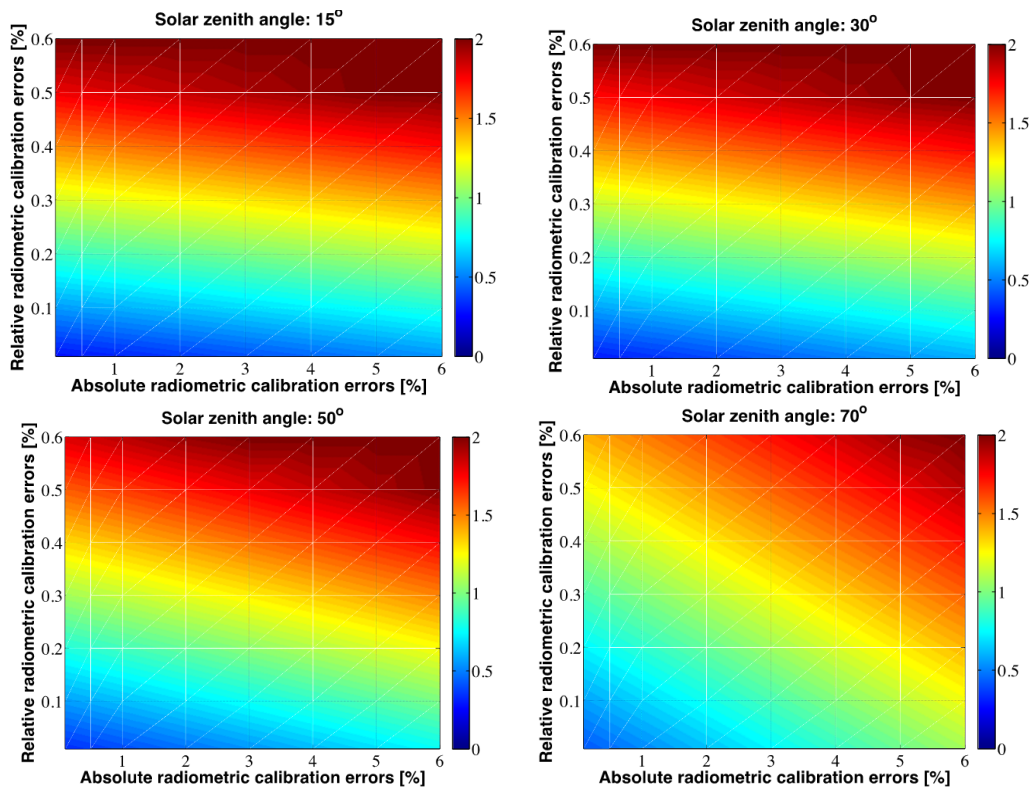


Figure. 1 The simulated nadir mode relationship between absolute and relative radiometric calibration accuracy and its impact on XCO₂ retrieval precision at different solar zenith angles of: (a) 15°, (b) 30°, (c) 50° and (d) 70°

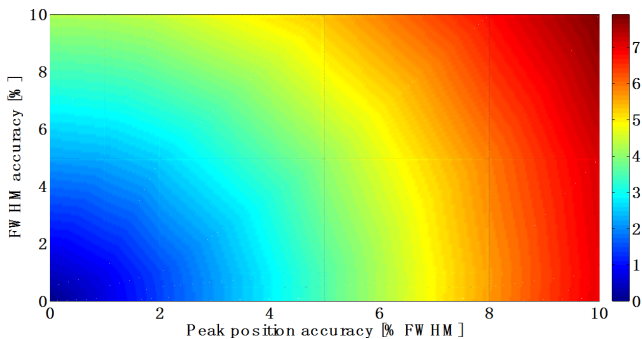


Figure. 2 The spectral calibration accuracy, such as (Full Width at Half Maxima) FWHM and Peak position, and its impact on XCO₂ retrieval precision with assumption of Gaussian Instrument Line Shape (ILS)

retrieval, although the O₂-A and CO₂ strong band is employed to constrain the aerosol amount and wavelength dependence. NASA OCO-2 flies in the A-Train^[7]. Therefore, other instruments also in the A-Train, such as the Cloud-Aerosol Lidar with Orthogonal Polarization (CALIOP) onboard Cloud-Aerosol Lidar and Infrared Pathfinder Satellite Observations (CALIPSO), Moderate Resolution Imaging Spectroradiometer (MODIS) onboard Aqua and Ozone Monitoring Instrument (OMI)

onboard Aura, can provide near-simultaneous measurements of clouds and aerosols for OCO-2. For GO-SAT, an auxiliary sensor, Cloud and Aerosol Imager (CAI), is onboard to screen out thick clouds contamination and reduce scattering-induced errors from aerosols and cirrus^[25-27]. For TanSat, a similar concept of a synergistic observation is required to improve the CO₂ measurement precision from the supplementary cloud and aerosol information. Therefore, the auxiliary instrument CAPI is designed and is located onboard TanSat. It observes the reflected sunlight in five bands from UV to NIR. In order to achieve more information on aerosol size, which affects the wavelength dependence of aerosol optical properties significantly, the CAPI includes two polarization channels that can measure the first three elements I, Q, U of the Stokes vector at 0.67 and 1.64 μm^[28]. In addition, a channel centered at 1.375 μm is employed for improving screening for cirrus.

A multi-spectral aerosol properties retrieval algorithm is developed for CAPI measurement^[29]. Based on empirically established relationships of surface reflectances at 1.64 μm and other bands in terms of the sur-

face Normalized Difference Vegetation Index (sNDVI), a fine model fraction (fmf), the surface reflectance at 0.67 μm and sNDVI is approached with total AOD (at 0.55 μm here in after) simultaneous. This algorithm has been tested using MODIS measurements and validated with Aerosol Robotic Network (AERONET) products, including a Root-Mean-Square Error (RMSE) of AOD about 0.16 at the Beijing and Xianghe sites, in August 2007. The retrieval precision is the same order of magnitude as the MODIS official product (RMSE = 0.14) during the same period^[30]. Additional information on aerosol optical properties provided by utilizing of CAPI polarization measurements is studied from a Bayes based linear analysis of OEM. The results prove that polarization observations of CAPI could help us obtain more information on AOD and the fraction of fine and coarse particles in aerosol retrieval^[31].

Based on previous studies^[23,32], the uncertainty in optical path length introduced by cloud and aerosol scattering could result in significant errors in CO_2 retrieval. Therefore, the aerosol properties simultaneously measured by CAPI are useful in compensating these CO_2 retrieval errors. According to the analysis of aerosol information content from simulated CAPI measurements^[31,33], we conducted further studies into the improvements of interference errors in XCO_2 after using aerosol information from CAPI observation.

In the CO_2 retrieval, the state vector (\mathbf{x}) includes the CO_2 mixing ratio profile (\mathbf{u}) and non- CO_2 parameters (\mathbf{e}), such as surface reflectance parameters, water vapor, and aerosol parameters. Each element of the state vector could cause smoothing and interference errors in the XCO_2 retrieval, as shown in Equation (2) below^[34],

$$\Delta\mathbf{X}_{\text{CO}_2} = \mathbf{h}^T (\hat{\mathbf{x}} - \mathbf{x}) = \mathbf{h}^T (\mathbf{A}_{\text{uu}} - \mathbf{I})(\mathbf{u} - \mathbf{u}_a) + \mathbf{h}^T \mathbf{A}_{\text{ue}} (\mathbf{e} - \mathbf{e}_a) + \varepsilon_u \quad (2)$$

The first and second term in this equation represent smoothing and interference error, respectively, and ε_u all other sources of error. Here \mathbf{A}_{uu} and \mathbf{A}_{ue} are submatrices of the averaging kernel matrix \mathbf{A} , describing the CO_2 -only component and those which mix elements of the CO_2 profile \mathbf{u} and the non- CO_2 elements \mathbf{e} , respectively. The subscript a represents the a priori, and \mathbf{I} is the identity matrix. \mathbf{h} is the pressure weighting function relating the CO_2 profile on each pressure level to the profile-weighted average XCO_2 , which means $\text{XCO}_2 = \mathbf{h}^T \hat{\mathbf{x}}$. In our study, we only focused on the interference

error (the second term in Equation 2) from aerosol parameters. The interference error (σ_{int}) can be calculated as follows,

$$\sigma_{\text{int}}^2 = \mathbf{h}^T \mathbf{A}_{\text{ue}} \mathbf{S}_{\text{ec}} \mathbf{A}_{\text{ue}}^T \mathbf{h} \quad (3)$$

where \mathbf{S}_{ec} indicates the error covariance matrix of the aerosol parameter. The averaging kernel \mathbf{A} can be calculated based on the a priori error covariance matrix \mathbf{S}_a , weighting function \mathbf{K} and measurement error covariance matrix \mathbf{S}_ε as follows,

$$\mathbf{A} = (\mathbf{K}^T \mathbf{S}_\varepsilon^{-1} \mathbf{K} + \mathbf{S}_a^{-1})^{-1} \mathbf{K}^T \mathbf{S}_\varepsilon^{-1} \mathbf{K} \quad (4)$$

To simulate the effect of CAPI aerosol measurements on CO_2 retrieval, we compared the interference error from all aerosol parameters before and after using CAPI observations. From our previous study^[31], the uncertainties of aerosol properties could be reduced from CAPI measurements. Thus, we used the a priori error and the posteriori error of aerosol parameters based on simulated CAPI observation to construct the diagonal matrix \mathbf{S}_{ec} , before comparing the improvement of interference errors in XCO_2 . Considering that the aerosol information from CAPI mainly focused on the total volume concentration and volume fmf (fmf_v) of the aerosol, we only changed the uncertainties of these two parameters in our comparison. The change in the difference of interference error in XCO_2 is shown in Figure 3, with fmf_v increased from 0.1 to 0.9 and AOD from 0.1 to 1.0. From Figure 3a–b and 3d–e, the uncertainties of aerosol parameters could cause 0.2–0.3 ppm interference error in the XCO_2 , while the error is always larger over lower surface reflectance due in part to the relative larger impact of aerosol scattering on lower reflectance signal. Figure 3c and 3f show 0.002–0.005 ppm improvement in the aerosol interference error when the aerosol uncertainty is reduced by CAPI measurements. Although the reduced error in XCO_2 is not large compared with CO_2 retrieval precision requirement, this improvement is largely related to aerosol types. Generally, the improvement becomes significant when the AOD increases. Furthermore, this improvement also varied with fmf_v and becomes more significant if the atmosphere is heavy polluted by small particles. Therefore, the use of CAPI in observations could provide more information on aerosol and reduce the XCO_2 error when AOD is large.

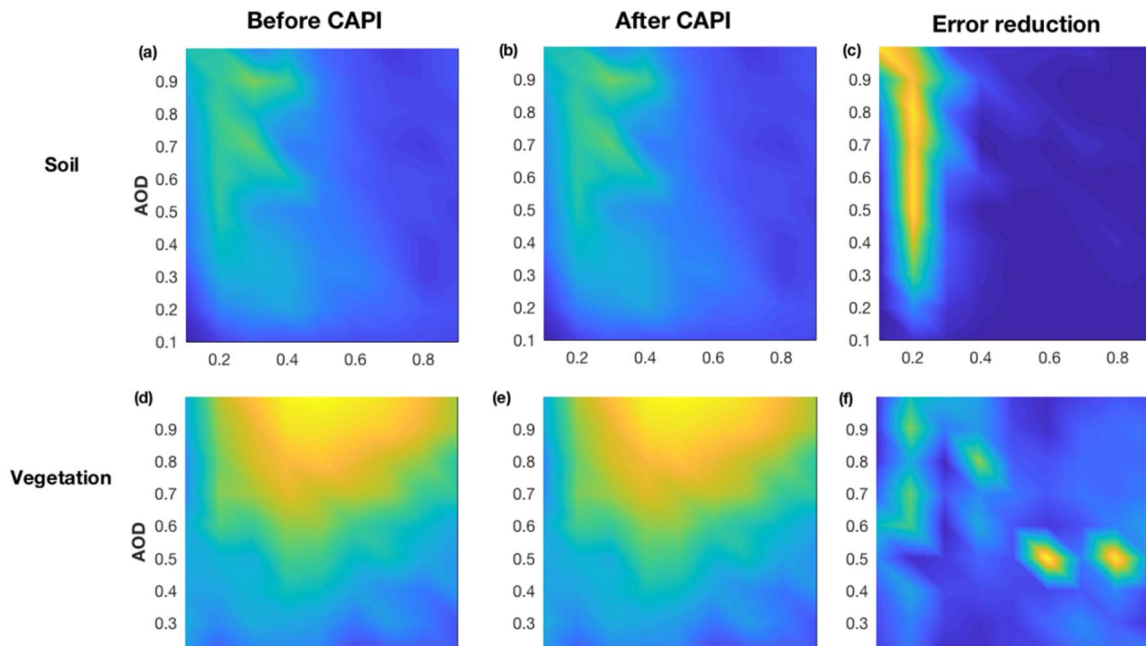


Figure 3 The aerosol induced interference errors in XCO_2 varying with aerosol optical depth (AOD) and fine mode fraction (fmf) over soil (the first row) and vegetation surface (the second row). (a) and (d) are interference errors before using aerosol information from CAPI simulated measurements. (b) and (e) are results after using CAPI measurements. (c) and (f) are error reductions between them

2.2 Retrieval Algorithm Development

Previous studies have shown a significant influence of the atmospheric and surface status on the spectra received at the top of the atmosphere [35,36], which can induce errors in retrieval. A full physical algorithm is appropriate for deriving XCO_2 due to the simulation of radiative transfer on a physical basis. An XCO_2 retrieval algorithm was developed and named after the Institute of Atmospheric Physics, Chinese Academy of Science (IAPCAS), to support the TanSat mission. A modification version was introduced as an application of the TanSat algorithm on GOSAT observations (ATANGO) [37]. Validation with Total Column Carbon Observing Network (TCCON) [38] measurements indicated that only a 1% (4 ppm) error remained in XCO_2 retrieval, which will thus serve as the TanSat operational algorithm.

Recently, some improvements to the IAPCAS algorithm have been made based on a previous version, which includes the modification of radiative transfer calculations, aerosol parameters, and retrieval strategy. The GOSAT Level 1B (L1B, measured spectrum) data were used in the retrieval experiments. Nine TCCON sites at different latitudes and on different continents were selected for the validation study. Most of the validation bias was better than 1 ppmv, while most of the

Root-Mean-Square Deviation (RMSD) was better than 2 ppmv [39]. Statistical data from all validation sites had a bias of 0.15 ppmv and an RMSE of 1.48 ppmv, which is sufficiently accurate for the study of carbon fluxes [40].

An algorithm for retrieving surface pressure from hyper-spectral measurements in oxygen A-bands has been developed and will be applied to TanSat surface pressure retrievals [41]. Methane (CH_4) is the second most important GreenHouse Gas (GHG). Based on GOSAT data, sensitivity studies have demonstrated the possibility of CH_4 retrieval in the Short-Wavelength Infrared (SWIR) band and have shown that the 1.65 μm band, which is associated with the 2.06 μm CO_2 band, retains more than 90% of the CH_4 and CO_2 content information [42].

The final product of TanSat will be the CO_2 flux at the regional and global scales. To derive the CO_2 flux from XCO_2 , we have developed a novel framework (TanTracker) for assimilating observations of atmospheric CO_2 concentrations, which is based on the POD-based ensemble four-dimensional variation data assimilation method (PODEn4DVar). An experiment for assimilating the real dry-air column CO_2 retrievals (XCO_2) from the Japanese GOSAT further demonstrated its potential for numerous applications [43,44]. ATANGO product has been used in carbon flux inversion in China,

and the result indicates a large error reduction of 84% on annual carbon flux when compared with in situ–only inversion^[40].

3. Scientific Requirements Investigation

3.1 Observation System Simulation Experiments

Observation System Simulation Experiments (OSSEs) are an efficient way to really describe space-borne measurement before the satellite launch. The main object of OSSE is to evaluate how the measurement improved the current knowledge on the object, e.g. CO₂ fluxes. An Ensemble Kalman Filter (EnKF)-based ensemble data assimilation system has been developed to simultaneously assimilate the consecutive XCO₂ observation and has been applied in the assessment of OCO measurements^[12]. In this system, the posterior state vector \mathbf{x}^a is improved from the prior state vector \mathbf{x}^f at each assimilation cycle via:

$$\mathbf{x}^a = \mathbf{x}^f + K \left[\mathbf{y} - H(\mathbf{x}^f) \right] \quad (5)$$

where H is observation operator that makes the correlation between surface CO₂ flux and observations. This improvement on the state vector is decided from the difference between the measurement \mathbf{y} and simulation $H(\mathbf{x}_a)$ and their uncertainties by a Kalman gain matrix \mathbf{K} :

$$\mathbf{K} = \mathbf{P}^f \mathbf{H}^T \left[\mathbf{H} \mathbf{P}^f \mathbf{H}^T + \mathbf{R} \right]^{-1} \quad (6)$$

where \mathbf{P}^f and \mathbf{R} is the a priori and observation error covariance, respectively; \mathbf{H} is Jacobin of observation operator \mathbf{H} ; and \mathbf{R} is the diagonal including instrument error, retrieval error, model error and representation error^[45]. In this study, we assumed that there was a uniform error over land (2.5 ppmv) and ocean (1.5 ppmv)^[12,45], respectively for the last two types of error. Instead of approaching the monthly surface flux, we do the inversion by calculating a scale factor coefficient on a priori surface flux of 144 regions globally, which included 99 land regions, 44 ocean regions, and a zero-emission region^[12,46]

The observation operator H is obtained from a Chemistry Transport Model (CTM) GEOS-Chem (v9-02) at a horizontal resolution of 4.0° (latitude) × 5° (longitude) with 47 vertical levels, which span from the surface to the mesosphere with typically 35 levels in the troposphere. The GEOS-Chem is driven by GEOS-5 meteorological analyses from the NASA Goddard Global Modelling and Assimilation Office. A priori flux in-

ventories are composed of a three-hour flux for the terrestrial biosphere^[47], monthly ocean flux^[48], monthly biomass burning fluxes (GFED v3.0)^[49] and monthly fossil fuel emissions^[50].

The OSSE system includes two major parts: generating pseudo-observations by sampling and screening the model atmosphere and using an ETKF approach to assimilate simulated observations to evaluate their impacts. To generate the pseudo-TanSat XCO₂ measurement, we sampled GEOS-Chem 3-D field of CO₂ concentrations at the time and the location of each nadir and glint measurement in the TanSat orbit. We used 3-hour European Centre for Medium-Range Weather Forecasts (ECMWF) Probability Density Functions (PDFs) of the cloud to remove cloudy scenes as well as Aerosol Optical Depths (AOD), derived from the MODIS instruments^[16], to remove aerosol contamination (AOD > 0.3) scenes. Finally, we mapped the 1-D CO₂ concentration profiles according to Connor *et al* (2008)^[34] with TanSat scene-dependent averaging kernels. The observation retrieval uncertainties are calculated as a function of surface type, solar zenith angle, aerosol optical depth and measurement mode (nadir or glint) using the full-physics ATANGO scheme. To control the quality of observations, only the nadir mode with SZAs in the range of 10°–85° and the glint mode with SZAs in the range of 10°–72° are recognized as realistic measurements in this study.

Then we use the generated observations to estimate regional flux with ENKF method. A 5-month lag window is used to reduce computational costs incorporated by the sequential data assimilation technique to digest observations step by step.

3.2 Contribution of TanSat Measurement to Flux Inversion

We evaluated the TanSat measurements using the OSSE framework and EnKF approach. The OSSE has been extensively used in satellite measurement optimization studies in order to investigate the impact of a measurement on data assimilation. For our study, we used a natural run to generate satellite observations. In the natural run, we calculated the regional fluxes using flux inventories and the results are used as ‘true’ values to generate satellite observations. Then, we designed an assimilation run to assess the effect of satellite measurements. In the assimilation run, the ‘true flux’ was multiplied by a factor of 1.8 as the prior flux and multiplied by 0.3 as the

prior uncertainties.

In order to investigate the performance of assimilation, we use error reduction γ to evaluate the change of uncertainties:

$$\gamma = 1 - \sigma^a / \sigma^f \quad (7)$$

where σ^a and σ^f denote the posteriori and a priori variance uncertainties, respectively. For each month in a certain region, we calculated σ^f from the a priori error covariance when it first enters the lag window and σ^a from the posteriori error covariance when it leaves the lag window.

The error reduction of assimilation run with TanSat orbit (mode B) in January, April, July, and October are shown in Figure 4. The results indicate a strong seasonal dependence over middle and high latitude regions both in the northern and southern hemisphere. Over the northern hemisphere, the uncertainty reduction is very limited in January, especially when the latitude is greater than 50°N. However, error reduction in these regions reached to more than 80% in July. The three northern hemisphere regions located in high latitude between 50°N–70°N,

including North American Boreal, Eurasia Boreal, and Europe, show the most obvious seasonal dependence. This is because the quantity and quality of satellite measurements in middle and high latitude regions with both nadir and glint modes are depend on seasons. These regions have more effective measurements in summer. We can also find regions that are relatively independent with the season, such as South American Tropical, North Africa, South Africa and Tropical Asia. In those regions, the satellite measurements are significantly affected by cloud contamination in the wet season and smoke aerosol in the dry season.

3.3 Optimal Design for TanSat

In the initial stage, TanSat was designed to operate in a 32-day cycle with a 16-day nadir mode and 16-day glint mode. In fact, there are no ocean measurements recorded in 16-day nadir mode, which means the data continuity will be interrupted. This is defective because regional CO₂ concentration is able to vary obviously in this ‘no data’ period due to the seasonal variation and unpredictable anthropic emissions.

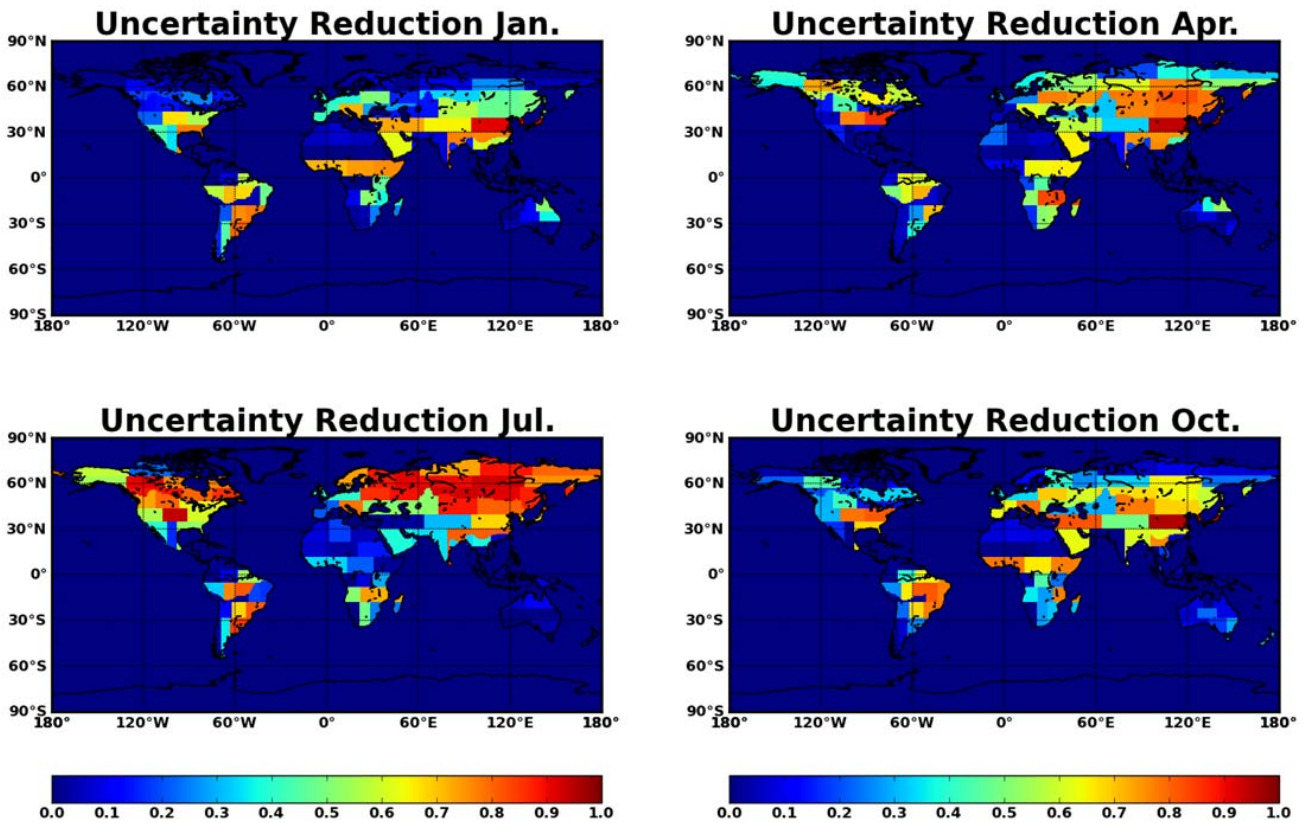


Figure 4 The error reduction of TanSat (mode B: one glint orbit and one nadir orbit) in the different seasons: (a) January, (b) April, (c) July and (d) October, respectively

In this study, we evaluated the potential impact of observation spatial coverage and frequency on land flux inversion in a top-down approach. In order to investigate the optimal TanSat operational duty cycle, we employed a set of comparison experiments in a 32-day cycle of 2009. There are four tests (Table 1), including (A) 16-day nadir mode +16-day glint mode; (B) alternative observation mode with one nadir mode orbit and one glint mode orbit; (C) intelligent selection with nadir mode over land and glint mode over ocean; and (D) only nadir mode observation.

Flux bias (posteriori flux-prior flux) and monthly mean error reduction of our designs are given in Table 2. The only nadir observation (D) is the worst choice be-

cause the measurement over the ocean can interpret the flux both in the ocean and over land that is located upstream of the ocean region. Aside from the only nadir mode, the other three modes have a similar error reduction. The intelligent selection mode (C) needs extended technical requirements in both mechanics and calibration because the satellite needs to adjust continually during the flight. The TanSat operates in mode B now, but this strategy may be optimized further in the future. The OCO-2 was optimized on November 12, 2015 with a new observation scheme similar with mode (C). The change was made on the 72 almost entirely over ocean orbits, these orbits will be always measured in glint mode.

Table 1 TanSat Observation Experiments System Simulation Description

Experiment	Description
TanSat only measurement	
A	16-day nadir (only land) + 16-day glint
B	One nadir orbit (only land) + one glint orbit (TanSat may use this)
C	A flexible instrument, change observation mode depend on the surface character (nadir mode over land and glint mode over ocean)
D	16 nadirs (only land)
Two satellites constellation observation measurement	
E	Use almost the same orbit, but the opposite measurement mode (one use nadir mode when another one use glint mode), so this method can get the most effective observations at the same time
F	16-day nadir+16-day nadir (one satellite's orbit is between the other one's two adjacent orbits)

Table 2 Results of different measurement designs for the land regions of 2009

Experiment	Land flux bias (GtC/yr)	Monthly mean Error reduction
A	0.35	63%
B	0.33	64%
C	0.26	65%
D	0.66	57%
E	0.22	71%
F	0.45	64%

Before TanSat was launched, there are three greenhouse gas satellites in space (GOSAT, OCO-2, and TanSat), and more satellites are on the way, such as GOSAT-2 and OCO-3. TanSat and OCO-2 have similar instrument designs, operating orbits and scan modes. The joint observation could provide at least double coverage or repetition of a single flight measurement. Therefore, we should consider the collaboration of satellite observations as a double satellite constellation. Two joint observation schemes have been tested with our OSSE

framework. The complementary observation mode (E) means two satellites use different observation modes (one uses nadir mode when the other one uses glint mode). The other intensive observational mode (F) means two satellites using the same observation mode. The complementary mode (E) could provide additional measurements over the ocean (or land) when the over land (ocean) measurement is in operation. The results indicate that the complementary mode has more contribution than the intensive mode with a larger error reduction and more consistent with the 'true flux'. Actually, the intensive mode does not provide a considerable amount of extra information to flux inversion. The difference between E and F is that the complementary mode increases the repetition frequency and the intensive mode increases the coverage. The results indicate that the frequency of measurements is very important in satellite observation design and should be considered carefully, especially in high-density and narrow swath grading spectrometers, such as OCO-2 and TanSat. With two

satellites (mode E), we have a larger error reduction (7%) and a smaller post flux bias.

4. Preliminary Results and Validations

4.1 Preliminary Global XCO₂ Retrieval and Seasonal Variation

In the TanSat XCO₂ retrieval algorithm that is developed from the IAPCAS platform (Liu *et al.*, 2013; Yang *et al.*, 2015), apart from CO₂ VMR, several other geophysical variables are retrieved, including the H₂O scale, temperature shift, surface pressure, aerosol optical properties and vertical distribution, cirrus optical properties and vertical distribution, Solar Induced Fluorescence (SIF), as well as wavenumber dispersion for each band and surface reflectance, are also included in the state vector list. The forward model has been updated from scalar version of ATANGO used to a vector version that could be utilized for OCO-2 and TanSat retrieval. We use 11 years' CarbonTracker-2013 data to develop a latitude belt in advance for CO₂ VMR and covariance. In order to extract the maximum amount of information from measurements, we enlarged the covariance matrix to be 10 times larger, which provides a loose constraint on CO₂ VMR. The a priori of atmospheric background, including temperature, water vapor, and pressure, was obtained from CMA T639 forecasts gridding data. Aside from ATANGO, recently, we also have applied the TanSat algorithm in OCO-2 measurements. This preliminary study indicates that the inter-comparison is -0.25 ± 1.39 ppm when compared with the OCO-2 v7r bias-corrected data in January 2015 at the global scale.

TanSat L1B v1.0 data is used to approach the XCO₂ in this study. Due to the CAPI still being in the on-orbit calibration, we used the O₂-A band to screen out cloud contamination from two narrow sub-bands on the P and R branch, which is insensitive to temperature variation. The TanSat spectrum involves only one direction of polarization incidental light. The simulated spectrum that is computed from the forward model needs to be converted into measurements by the Stokes coefficients. The radiometric calibration of TanSat records the relationship from the received DN and incident radiance before polarizer. Therefore, the stokes convert function is:

$$I_{\text{measurement}} = I + \cos(2\theta) \cdot Q + \sin(2\theta) \cdot U \quad (8)$$

where I , Q and V represent first three Stokes parameters; and θ is the polarization angle that is defined as the an-

gle between the local meridian plane and principal plane. The transfer essentially means that the rotation of radiance from local meridian plan to the measurement direction in the principal plane.

The first 6-months of TanSat measurement shows a seasonal decrease of around 5-8 ppm in XCO₂ from late winter (Feb.) to mid-summer (Jul.) in the Northern Hemisphere, which is a result mainly from a change in the rate of photosynthesis^[51,52]. Emission hotspots due to anthropogenic activity, such as industrial activity and fossil fuel combustion, are clearly evident in eastern China, the eastern United States, and Europe from Feb. to May in Northern Hemisphere^[53]. We can also figure out there is high concentration band around rainforests and Veld of Africa below the Sahara, which can show the seasonal burning in this region in dry season^[54]. The XCO₂ gradient is indicated between the Northern Hemisphere and Southern Hemisphere obviously.

4.2 Inter-comparison with OCO-2 Measurement

In order to validate the TanSat XCO₂ retrieval, we compared with OCO-2 measurement in an overlap observation orbit. TanSat flies in a ~700 km sun-synchronous orbit, which is similar to OCO-2. Due to the differences in orbit altitude, pass time and inclination, two satellites usually have a different footprint distance. Fortunately, there is an overlap footprint observation on 20 April 2017, which provides an opportunity to inter-compare the retrieval results. We selected the observation over the north Australia of orbit 01739 of TanSat and orbit 14896 of OCO-2. OCO-2 and TanSat show a retrieval on a similar level of 395–410 ppm. The statistical results of TanSat (OCO-2) indicate an average of 400.78 ppm (OCO-2: 400.38 ppm) and 397.38 ppm (OCO-2: 399.16 ppm) in the north and south sub-region, respectively, and the difference is 0.4 and -1.78 ppm in north and south region respectively.

4.3 Validation Against TCCON

The ground-based measurements such as The Total Carbon Column Observing Network (TCCON) (Wunch *et al.*, 2012) has been accepted as a standard for validating XCO₂ estimates retrieved from satellite measurement and has been applied in GOSAT and OCO-2 validation. TanSat has an 18 km nadir swath, which means the exact coverage by the TCCON station is difficult. Therefore, we evaluate and validate the preliminary TanSat results against TCCON measurement collected within ± 2 hours

around satellite measurement in 550 km distance region was selected in validation experiment. The error of retrieval was calculated by minus the ± 2 hour mean of TCCON measurement, from a validation experiment near the Sodankyla (Finland) ^[55,56] of TCCON station. There are 4 orbits (15 Feb., 19 Feb., 26 Feb. and 2 Mar), which passed the neighborhood area around the site during 15 February–15 March 2017 and were not seriously contaminated by the cloud. All retrieved data have been double checked by the MODIS/Aqua cloud product. The statistic indicates an average of 405.43 ppm from TanSat measurements and 407.62 ppm for TCCON observations.

In additional, TanSat XCO₂ estimates collected near 9 TCCON sites were selected in TanSat validation, including Pasadena, JPL, Lamont and Park Falls in the U.S., East Trout Lake in Canada, Saga in Japan, Lauder in New Zealand and Sodankyla in Finland. In this study, we only validate the retrieval from nadir mode measurement. Basically, almost all the results fall within 1% (~4ppm) region that is marked by dotted grey lines and error bars that indicate the precision is less than 1%, which means the preliminary results has met the TanSat mission accuracy and precision design requirements. TanSat XCO₂ has a better agreement with Lamont, Park Falls, East Trout Lake than others. We found large errors in Saga and Pasadena in spring and Sodankyla though the first 6 months of observation. JPL and Lauder show a relatively small error. However, due to TanSat's narrow swath, long repeat time and cloud contamination, the matchup data is too limited to support a further analysis. The average precision for each month is around 2 ppm, March shows the worst value of 3.35 ppm and may show the best value of 1.67 ppm.

5. Outlook and Conclusions

Since TanSat mission started in 2011, the TanSat team has completed the following stages in order to meet the observation scientific requirements: (1) Design, manufacture and integration of instruments and satellites; (2) investigations of scientific requirement and capability; (3) development and implementation of XCO₂ retrieval algorithm and CO₂ flux inversion system; (4) laboratory characterization and calibration of radiometric and spectral performance; (5) surface calibration and validations in addition to determining a plan for a validation campaign. After the successful launch of TanSat in De-

cember 2016, the data will be widely used in scientific research and applications by science teams and government agencies.

In this paper, we show the preliminary results on XCO₂ retrieval from TanSat measured spectrum and validation of retrieval XCO₂ against TCCON measurement. The first 6-month nadir measurements over land indicate the XCO₂ variation from northern hemisphere winter to summer and also the latitude gradient. The photosynthesis from vegetation significantly reduces XCO₂ in June and July, especially for emission hot spot from anthropogenic activity in eastern China, the eastern United States, and Europe, which can be clearly distinguished from Feb. to May. Validation against TCCON indicates that TanSat has met the precision design and an average of 2.11 ppm with the best of 1.67 and worst of 3.35 ppm. In a future study, the improvement of on-orbit calibration will provide more accurate measurements to improve the XCO₂ retrieval quality and precision.

Measurement precision, spatial coverage, and sampling repeat impact the uncertainty reduction in flux inversion significantly. In the TanSat OSSE study, we show the observations of two satellites and compared these with a single satellite to indicate that an extra 10% reduction in the flux uncertainty if the measurement of complementary satellites has no bias and similar precision. In order to meet the scientific requirement of carbon flux inversion, therefore, we need accurate optimal joint measurement to obtain more data to reduce uncertainty in flux inversion. There will be more greenhouse gas satellites joining the family in the future, and the joint measurements will provide more valuable data to global greenhouse gas cycle investigation.

Acknowledgments This work was supported by National Key R&D Program of China (2016YFA0600203), the National High-tech Research and Development Program (2011AA12A104), External Cooperation Program of the Chinese Academy of Sciences (Grant No. GJHZ1507) and National Key R&D Program of China (2017YFB0504000). We thank TanSat team member, Yonghe Zhang, Wu Liu from Shanghai Engineering Center for Microsatellites, Chinese Academy of Sciences, Peng Zhang, Zhongdong Yang, Yanmeng Bi, Qian Wang and Ronghua Wu from National Satellite Meteorological Center, China Meteorological Administration, Yuquan Zheng, Changxiang Yan and Chao Lin from Changchun Institute of Optics, Fine Mechanics and Physics, Chinese

Academy of Sciences, Minzheng Duan and Xiangjun Tian from Institute of Atmospheric Physics, Chinese Academy of Sciences, Chengcai Li from Peking University, and the people working in TanSat mission. The authors thank Dr. Liang Feng in University of Edinburgh to provide the PyOSSE and Sodankyla station provide in-situ measurement data, OCO-2 team provide satellite product, TCCON research team for TCCON CO₂ data, Prof. Hartmut Boesch and Dr. Johanna Tamminen for the valuable discussions, science team of GOSAT, SCHI-AMACHY, RemoTeC (SRON and KIT) and OCO-2 team for the valuable suggestions.

References

- [1] Bovensmann H, Burrows JP, Buchwitz M, *et al.* Sciamachy: Mission objectives and measurement modes. *Journal of the Atmospheric Sciences*, 1999, 56: 127-150
- [2] Bösch H, Toon G C, Sen B, *et al.* Space-based near-infrared CO₂ measurements: Testing the orbiting carbon observatory retrieval algorithm and validation concept using sciamachy observations over park falls, wisconsin. *Journal of Geophysical Research: Atmospheres*, 2006, 111 (D23): 5495-5513
- [3] Heymann J, Reuter M, Hilker M, *et al.* Consistent satellite CO₂ retrievals from sciamachy and gosat using the besd algorithm. *Atmospheric Measurement Techniques*, 2015, 8: 2961-2980
- [4] Yokota T, Yoshida Y, Eguchi N, *et al.* Global concentrations of CO₂ and CH₄ retrieved from gosat: First preliminary results. *Sola*, 2009, 5: 160-163
- [5] Kuze A, Taylor TE, Kataoka F, *et al.* Long-term vicarious calibration of gosat short-wave sensors: Techniques for error reduction and new estimates of radiometric degradation factors. *IEEE Transactions on Geoscience and Remote Sensing*, 2014, 52: 3991-4004
- [6] Yoshida Y, Kikuchi N, Morino I, *et al.* Improvement of the retrieval algorithm for gosat swir CO₂ and CH₄ and their validation using tcccon data. *Atmospheric Measurement Techniques*, 2013, 6: 1533-1547
- [7] Eldering A, amp, apos, *et al.* The orbiting carbon observatory-2: First 18 months of science data products. *Atmospheric Measurement Techniques Discussions*, 2016, 1-30
- [8] Crisp D, Pollock HR, Rosenberg R, *et al.* The on-orbit performance of the orbiting carbon observatory-2 (oco-2) instrument and its radiometrically calibrated products. *Atmospheric Measurement Techniques*, 2017, 10: 59-81
- [9] Boesch H, Baker D, Connor B, *et al.* Global characterization of CO₂ column retrievals from shortwave-infrared satellite observations of the orbiting carbon observatory-2 mission. *Remote Sensing*, 2011, 3: 270-304
- [10] Chevallier F, Engelen RJ, Carouge C, *et al.* Airs-based versus flask-based estimation of carbon surface fluxes. *Journal of Geophysical Research-Atmospheres*, 2009, 114:
- [11] Chevallier F, Feng L, Boesch H, *et al.* On the impact of transport model errors for the estimation of CO₂ surface fluxes from gosat observations. *Geophysical Research Letters*, 2010, 37:
- [12] Feng L, Palmer PI, Boesch H, *et al.* Estimating surface CO₂ fluxes from space-borne CO₂ dry air mole fraction observations using an ensemble kalman filter. *Atmospheric Chemistry and Physics*, 2009, 9: 2619-2633
- [13] Chevallier F, Breon F-M, Rayner PJ. Contribution of the orbiting carbon observatory to the estimation of CO₂ sources and sinks: Theoretical study in a variational data assimilation framework. *Journal of Geophysical Research-Atmospheres*, 2007, 112:
- [14] Liu JJ, Bowman KW, Lee M, *et al.* Carbon monitoring system flux estimation and attribution: Impact of acos-gosat X-CO₂ sampling on the inference of terrestrial biospheric sources and sinks. *Tellus Series B-Chemical and Physical Meteorology*, 2014, 66:
- [15] Feng L, Palmer PI, Parker RJ, *et al.* Estimates of European uptake of CO₂ inferred from gosat X-CO₂ retrievals: Sensitivity to measurement bias inside and outside Europe. *Atmospheric Chemistry and Physics*, 2016, 16: 1289-1302
- [16] Baker DF, Boesch H, Doney SC, *et al.* Carbon source/sink information provided by column CO₂ measurements from the orbiting carbon observatory. *Atmospheric Chemistry and Physics*, 2010, 10: 4145-4165
- [17] Li ZG, Lin C, Li CL, *et al.* Prelaunch spectral calibration of a carbon dioxide spectrometer. *Measurement Science and Technology*, 2017, 28:
- [18] Zhang H, Zheng YQ, Lin C, *et al.* Laboratory spectral calibration of tansat and the influence of multiplex merging of pixels. *International Journal of Remote Sensing*, 2017, 38: 3800-3816
- [19] Geddes A, Bosch H. Tropospheric aerosol profile information from high-resolution oxygen a-band measurements from space. *Atmospheric Measurement Techniques*, 2015, 8: 859-874
- [20] Lin C, Li C, Wang L, *et al.* Preflight spectral calibration of hyperspectral carbon dioxide spectrometer of tansat. *Optics and Precision Engineering*, 2017, 25: 2064-2075
- [21] Liu Y, Cai Z, Yang D, *et al.* Optimization of the instrument configuration for tansat CO₂ spectrometer. *Chinese Science Bulletin (Chinese Version)*, 2013, 58: 2787
- [22] Wang Q, Yang ZD, Bi YM. Spectral parameters and signal-to-noise ratio requirement for tansat hyper spectral sensor to measure atmospheric CO₂. In: IM E, YANG S, ZHANG P. *Remote sensing of the atmosphere, clouds, and precipitation v. 2014*.
- [23] Butz A, Hasekamp OP, Frankenberg C, *et al.* Retrievals of atmospheric CO₂ from simulated space-borne measurements of backscattered near-infrared sunlight: Accounting for aerosol effects. *Appl Optics*, 2009, 48: 3322-3336
- [24] Guerlet S, Butz A, Schepers D, *et al.* Impact of aerosol and thin cirrus on retrieving and validating CO₂ from gosat shortwave infrared measurements. *Journal of Geophysical Research-Atmospheres*, 2013, 118: 4887-4905
- [25] Ajiro M, Kawazoe F, Yokota T. An update on gosat standard products at five and a half years after the launch. In: XIONG X, SHIMODA H. *Earth observing missions and sensors: Development, implementation, and characterization iii. 2014*.
- [26] Ishida H, Nakjima TY, Yokota T, *et al.* Investigation of gosat tanso-cai cloud screening ability through an intersatellite comparison. *Journal of Applied Meteorology and Climatology*, 2011, 50: 1571-1586
- [27] Taylor TE, O'Dell CW, O'Brien DM, *et al.* Comparison of cloud-screening methods applied to gosat near-infrared spectra. *IEEE Transactions on Geoscience and Remote Sensing*, 2012, 50: 295-309

- [28] Zhang JQ, Shao JB, Yan CX. Cloud and aerosol polarimetric imager. In: OJEDACASTANEDA J, HAN S, JIA P, *et al.* Selected papers from conferences of the photoelectronic technology committee of the chinese society of astronautics: Optical imaging, remote sensing, and laser-matter interaction 2013. 2014.
- [29] Shi G, Li C, Ren T. Sensitivity analysis of single-angle polarization reflectance observed by satellite. *Chinese Science Bulletin*, 2014, 59: 1519-1528
- [30] Shi GM, Li CC, Ren T, *et al.* Retrieval of atmospheric aerosol and surface properties over land using satellite observations. *Ieee Transactions on Geoscience and Remote Sensing*, 2015, 53: 1039-1047
- [31] Chen X, Yang D, Cai Z, *et al.* Aerosol retrieval sensitivity and error analysis for the cloud and aerosol polarimetric imager on board tansat: The effect of multi-angle measurement. *Remote Sensing*, 2017, 9: 183
- [32] O'Dell CW, Connor B, Bösch H, *et al.* The acos co₂ retrieval algorithm – part I: Description and validation against synthetic observations. *Atmospheric Measurement Techniques*, 2012, 5: 99-121
- [33] Chen X, Wang J, Liu Y, *et al.* Angular dependence of aerosol information content in capi/tansat observation over land: Effect of polarization and synergy with a-train satellites. *Remote Sensing of Environment*, 2017, 196: 163-177
- [34] Connor BJ, Boesch H, Toon G, *et al.* Orbiting carbon observatory: Inverse method and prospective error analysis. *Journal of Geophysical Research: Atmospheres*, 2008, 113: n/a-n/a
- [35] Cai Z, Liu Y, Yang D. Analysis of xco₂ retrieval sensitivity using simulated chinese carbon satellite (tansat) measurements. *Science China Earth Sciences*, 2014, 57: 1919-1928
- [36] Bi YM, Yang ZD, Gu SY, *et al.* Impacts of aerosol and albedo on tansat co₂ retrieval using the near infrared co₂ bands. In: IM E, YANG S, ZHANG P. Remote sensing of the atmosphere, clouds, and precipitation v. 2014.
- [37] Liu Y, Yang D, Cai Z. A retrieval algorithm for tansat xco₂ observation: Retrieval experiments using gosat data. *Chinese Science Bulletin*, 2013, 58: 1520-1523
- [38] Wunch D, Toon GC, Blavier JF, *et al.* The total carbon column observing network. *Philos Trans A Math Phys Eng Sci*, 2011, 369: 2087-2112
- [39] Yang DX, Liu Y, Cai ZN, *et al.* An advanced carbon dioxide retrieval algorithm for satellite measurements and its application to gosat observations. *Science Bulletin*, 2015, 60: 2063-2066
- [40] Yang DX, Zhang HF, Liu Y, *et al.* Monitoring carbon dioxide from space: Retrieval algorithm and flux inversion based on gosat data and using carbontracker-china. *Advances in Atmospheric Sciences*, 2017, 34: 965-976
- [41] Liu H, Duan M, Lü D, *et al.* Algorithm for retrieving surface pressure from hyper-spectral measurements in oxygen a-band. *Chinese Science Bulletin*, 2014, 59: 1492-1498
- [42] Deng J, Liu Y, Yang D, *et al.* Ch₄ retrieval from hyperspectral satellite measurements in short-wave infrared: Sensitivity study and preliminary test with gosat data. *Chinese Science Bulletin*, 2014, 59: 1499-1507
- [43] Tian X, Xie Z, Cai Z, *et al.* The chinese carbon cycle data-assimilation system (tan-tracker). *Chinese Science Bulletin*, 2014, 59: 1541-1546
- [44] Tian X, Xie Z, Liu Y, *et al.* A joint data assimilation system (tan-tracker) to simultaneously estimate surface co₂ fluxes and 3-d atmospheric co₂ concentrations from observations. *Atmospheric Chemistry and Physics*, 2014, 14: 13281-13293
- [45] Peylin P, Baker D, Sarmiento J, *et al.* Influence of transport uncertainty on annual mean and seasonal inversions of atmospheric co₂ data. *Journal of Geophysical Research-Atmospheres*, 2002, 107:
- [46] Chevallier F, Palmer PI, Feng L, *et al.* Toward robust and consistent regional co₂ flux estimates from in situ and spaceborne measurements of atmospheric co₂. *Geophysical Research Letters*, 2014, 41: 1065-1070
- [47] Olsen SC. Differences between surface and column atmospheric co₂ and implications for carbon cycle research. *Journal of Geophysical Research*, 2004, 109:
- [48] Takahashi T, Sutherland SC, Wanninkhof R, *et al.* Climatological mean and decadal change in surface ocean pco₂, and net sea-air co₂ flux over the global oceans (vol 56, pg 554, 2009). *Deep-Sea Research Part I-Oceanographic Research Papers*, 2009, 56: 2075-2076
- [49] van der Werf GR, Randerson JT, Giglio L, *et al.* Global fire emissions and the contribution of deforestation, savanna, forest, agricultural, and peat fires (1997-2009). *Atmospheric Chemistry and Physics*, 2010, 10: 11707-11735
- [50] Oda T, Maksyutov S. A very high-resolution (1 km x 1 km) global fossil fuel co₂ emission inventory derived using a point source database and satellite observations of nighttime lights. *Atmospheric Chemistry and Physics*, 2011, 11: 543-556
- [51] Morino I, Uchino O, Inoue M, *et al.* Preliminary validation of column-averaged volume mixing ratios of carbon dioxide and methane retrieved from gosat short-wavelength infrared spectra. *Atmospheric Measurement Techniques*, 2011, 4: 1061-1076
- [52] Crisp D, Fisher BM, O'Dell C, *et al.* The acos co₂ retrieval algorithm - part ii: Global x-co₂ data characterization. *Atmospheric Measurement Techniques*, 2012, 5: 687-707
- [53] Le Quere C, Andrew RM, Friedlingstein P, *et al.* Global carbon budget 2017. *Earth System Science Data*, 2018, 10: 405-448
- [54] Crutzen PJ, Andreae MO. Biomass burning in the tropics - impact on atmospheric chemistry and biogeochemical cycles. *Science*, 1990, 250: 1669-1678
- [55] Kivi R, Heikkinen P. Fourier transform spectrometer measurements of column co₂ at sodankyla, finland. *Geoscientific Instrumentation Methods and Data Systems*, 2016, 5: 271-279
- [56] Tukiainen S, Railo J, Laine M, *et al.* Retrieval of atmospheric ch₄ profiles from fourier transform infrared data using dimension reduction and memc. *Journal of Geophysical Research: Atmospheres*, 2016, 121: 10, 312-310, 327